Mineralogical Magazine, December 2006, Vol. 70(6), pp. 731–741

Letter

Fe(II)/Fe(III) 'green rust' developed within ochreous coal mine drainage sediment in South Wales, UK

J. M. Bearcock[1,*], W. T. Perkins[1], E. Dinelli[2] and S. C. Wade[3]

[1] Institute of Geography and Earth Sciences, University of Wales, Aberystwyth SY23 3DB, UK
[2] Bologna University, Piazza di Porta San Donato, 1, Bologna, I-40126, Italy
[3] Institute of Biological Sciences, University of Wales, Aberystwyth SY23 3DA, UK

ABSTRACT

'Green rusts' are a group of reduced Fe hydroxides with a pyroaurite-like structure. In a new occurrence, green rust is present as a 45–60 mm thick band which lies just below the surface (~4 mm) of an ochreous deposit at an abandoned coal mine site. The sample is characterized by the presence of μm-sized hexagonal crystals which have been identified from SEM imaging. Chemical analyses reveal an Fe(II):Fe(III) ratio which is close to the characteristic 2:1 ratio, and XRD analysis identifies the material by characteristic lattice spacings. The green rust layer also contains aragonite which is not present in the surrounding ochre. Green rusts are important as they have the potential to be used in water treatment.

Keywords: Green rust, coal mine, ochre, drainage, South Wales.

Introduction

The occurrence of Fe(II)/(III) hydroxides, termed 'green rusts', was first reported in a PhD thesis by Keller (1948, cited by McGill *et al*., 1975). Green rust can be represented by the general formula $[Fe^{2+}_4Fe^{3+}_2(OH)_{12}]^{2+}[A{\cdot}2H_2O]$ (after Drissi *et al.*, 1995) where *A* represents an anion which is either SO^{2-}_3, SO^{2-}_4, $2Cl^-$, $2Br^-$ or CO^{2-}_3. Green rusts have a pyroaurite-like structure (Stampfl, 1969; Taylor, 1973; Brindley and Bish, 1976). The ratio of Fe(II) to Fe(III) in naturally occurring green rust is known to vary between a maximum of 4:1 and a minimum of 2:1 (Schwertmann and Cornell, 2000) whilst a recent study by Ruby *et al.* (2006) has generated 'fully ferric green rust.' When exposed to air, green rusts oxidize rapidly; in our study the material showed a colour change from green-black to orange within minutes of exposure to the air.

Green rusts have been recorded from a wide variety of surface and near-surface environments. Examples include corrosion of steel, particularly in the marine environment (Refait *et al.*, 2003), and the corrosion of Fe^0 iron filings in permeable reactive barriers (PRBs) (e.g. Phillips *et al*., 2003*b*; Wilkin and McNeil, 2003; Kamolpornwijit *et al*., 2004; Kohn *et al*., 2005). In addition green rusts are found in hydromorphic gley soils (Bourrie *et al*., 2004; Genin, 2004), suboxic soils and sediments (Hansen *et al*., 1996; Bond and Fendorf, 2003; O'Loughlin *et al*., 2003), as an unstable precursor/ product of Fe (III) species (Genin, 2004; Ona-Nguema *et al*., 2004) and in bacterial cultures (Ona-Nguema *et al*., 2004).

Green rust chemistry and mineralogy have received renewed interest in recent years because, in anoxic environments, Fe oxides containing Fe(II) are important as redox buffers (Jiang *et al*., 2003). Green rust has been shown to reduce nitrates in soils (Hansen *et al.*, 1996). Choe *et al.* (2004) investigated the use of elemental Fe for the removal of nitrate from groundwater and found that green rust acted as an additional reducing agent. The fate of chromate in soils was shown by Bond and Fendorf (2003) to be partially controlled by green rusts. They demon-

* E-mail: jjb@aber.ac.uk
DOI: 10.1180/0026461067060360

strated that different green rust types reduce at different rates in the order $Cl > CO_3 > SO_4$, but had no bearing on the nature of the product. The reduction of chromate by green rusts produced highly stabilized phases. O'Loughlin *et al.* (2003) showed that suspensions of green rust were 'readily' able to reduce Ag(I), Au(III), Cu(II) and Hg(II) to sub-micron sized particles of their zero-valent metals.

Green rusts are usually present in small quantities such that the Fe content within a green rust layer in soils is only 2–3.9% (Refait *et al*., 2001) and in PRBs the green rust is only present as a corrosion product. In this study we report a 45–60 mm layer of green rust with an Fe content of 20%. To the authors' knowledge green rust has not been previously reported in such accumulations or from ochreous mine deposits, but there is one reported occurrence in stored ochre sludge from a water treatment plant (Koch and Mørup, 1991). In this paper we use chemical analyses, SEM images, XRD data and DTA/TG to characterize the green rust and report this unusual occurrence.

Site description/geology

The new occurrence of green rust is from a coal mine drainage site in the South Wales Coalfield, UK. This coalfield is an elongate, synformal structure of Carboniferous Coal Measures ~80 km east–west and ~35 km north–south (Fig. 1). The mine site is in the lower part of the Neath valley where the principal coal seam was the Rhondda number two seam. This is overlain by the Upper Coal Measures fluvial Pennant Sandstones, which contain minor un-worked coal seams. The Middle Coal Measures below the Rhondda number two

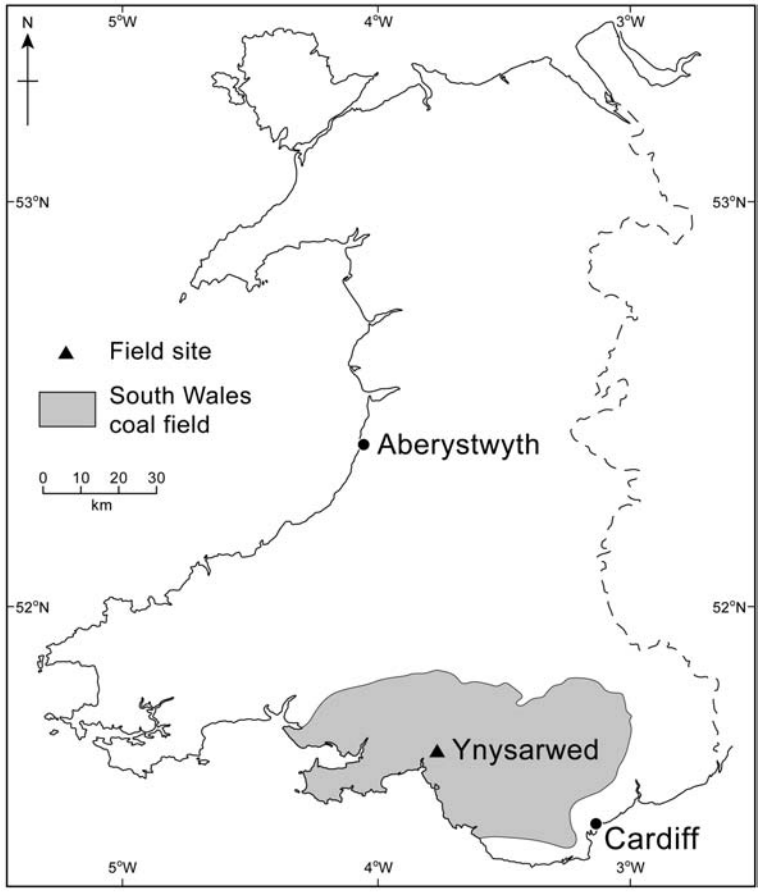

FIG. 1. Location of the Ynysarwed adit in the South Wales Coalfield, Wales, UK.

seam show a marked marine influence (Guion *et al*., 2000), which gives the coal in this area its high S content of between 2 and 4% of pyritic S (Evans *et al*., 2006).

The mine drainage site where the green rust has been identified is an adit at the former Ynysarwed coal mine site in the Neath Valley (SN 8061 0149). The Ynysarwed mine closed in 1938, causing occasional minor ferruginous discharge (Evans *et al*., 2006). The mine adit was maintained as an escape route for the adjoining Blaenant coal mine in the Dulais Valley, 2.5 km to the NW of the Ynysarwed adit, until the Bleanant mine closed in 1993 (Ranson, 1999). After the Bleanant mine closed, the water pumps in that mine were turned off and the mine flooded. The result of this flooding is that the Ynysarwed adit is the main drainage point for the abandoned mine complex. In the initial stages of flooding the adit released acidic Fe-rich waters directly into the Neath canal which turned 12 km of the canal orange/red with ochreous precipitation. The initial discharge was 'net acidic' with dissolved oxygen concentrations described as 'negligible' and an Fe content of >400 mg l^{-1} (Ranson, 1999).

Sampling and methodology

The sediment samples analysed in this study were collected from the entrance to the Ynysarwed adit. These sediments are precipitating naturally. The site currently consists of an arched brickwork entrance which is 1.3 m across, from which the discharge flows with a depth of ~10 cm above the accumulated ochreous sediment. The adit is fully flooded within ~2 m of the entrance. There is a thick ochreous deposit at the entrance to the adit, which has built up since the discharge began in 1993. This deposit is now ~1 m thick. The adit is protected by a metal grill, which is designed for safety and to prevent organic matter from clogging the flow but also restricts access for sampling the water and ochre.

Water samples were collected from the mine discharge and several cores were taken through the accumulated ochre. Water sampling followed standard procedures (McCleskey *et al*., 2004). The cores were extracted using a section of 50 mm internal diameter ABS (acrylonitrile-butadiene-styrene) waste pipe. After collection, the core was sealed with a layer of low-density polyethylene film and the remaining gap was filled with commercial expandable filler. The cores were kept cold (4ºC) and dark.

One of the cores was opened by cutting most of the way through the plastic pipe with a small circular saw. The core was cut into two sections using fine stainless steel wire and then separated using two stainless steel plates. The thickness of the layers was recorded and the core was immediately photographed. Once the core was split, the surface of the sediment was covered with low-density polyethylene film which was only temporarily removed to allow samples to be taken. All chemical analyses were carried out rapidly (within 2 h) to minimize the effects of oxidation.

The core was sub-sampled using a stainless steel spatula. Two types of sample were prepared. One set of samples was processed immediately for chemical parameters whilst the other set was prepared for scanning electron microscopy (SEM), X-ray diffraction (XRD) and differential thermal analysis/thermogravimetric (DTA/TG) work.

Chemical analyses for Fe were produced by sub-sampling with a ~3 mm resolution. Fe(II) was determined by titrimetric analysis, using a modification of the Wilson method (Wilson, 1955). In this method, sub-samples of the freshly opened core material were divided into two and quickly transferred to conical flasks and weighed. One of the sub-samples was treated with a solution of ammonium metavanadate and then digested with concentrated HCl. Once digestion of the ochre or green rust was complete, the excess ammonium metavanadate was titrated against standardized ammonium ferrous sulphate solution to determine Fe(II) concentration. The second sub-sample was dried and re-weighed to determine the water content. The Fe (total) concentration was determined by AAS following digestion of the second sub-sample using HCl. Fe(III) was calculated by subtraction. All chemical reagents used were of AnalaR grade. Blanks were prepared for each digestion method and duplicates were analysed where there was sufficient material. The precision of the AAS measurements was typically within 3% whilst the Fe(II) determinations were within 15%.

The core was subdivided into samples for analysis by SEM, XRD and DTA/TG. The sampling was designed to represent the distinct colour changes observed in the core. Where the individual layers were thick enough, they were subdivided with a 1 cm resolution. Each SEM sub-sample was air dried and then disaggregated using an agate mortar and pestle. Sample powders

were then mounted for SEM analysis by sprinkling the powder onto double-sided sticky tape attached to an SEM stub. The samples were sputter-coated with a 4 nm layer of Pt/Pd. Scanning electron microscopy images were obtained using an Hitachi S-4700 Field Emission SEM instrument in the Institute of Biological Sciences, Aberystwyth, Wales. Images were collected with either the secondary electron detector or the back-scattered electron detector. The key operating conditions (such as accelerating voltage, working distance and detector type) for each image is shown on the image and the information is presented in the figure caption.

Bulk sub-samples through the core were analysed by XRD at the University of Bologna. Powder was placed into alumina holders to avoid introducing preferential orientation of the sample. The samples were analysed using a Philips PW 1710 equipped with a Cu tube, with spinner and secondary monochromator giving an X-ray wavelength of 1.54056 Å. The step size was 0.02º2θ and the scan rate was 2.5 s per step. Samples were also prepared for DTA/TG at the University of Bologna. Thermal analyses were performed on 30 mg of sample powder using a Setaram TAG24 double furnace system with simultaneous registration of TG and DTA data. The heating rate was 20ºC min^{-1}, and measurements were carried out under a CO_2 flux. A blank was subtracted for each run in order to compensate for possible instrumental drift.

Results

The layering in the core is illustrated in Fig. 2 and the chemical changes are listed in Table 1. The top layer (~4 mm thick) is red in colour (Munsell 10R 4/8) and is very loosely consolidated. This layer represents the material that is precipitated within the drainage adit. The green rust layer is found immediately below this layer, and is a distinctly green-black layer (Munsell Gley1 2.5/2 – very dark greyish green). The green rust layer has a much firmer texture and is 45–60 mm thick, below which the ochre becomes predominantly red (Munsell 2.5YR 5/8) in colour to a depth of ~210 mm. Both the upper and lower boundaries of the green rust layer are very abrupt in both colour change and texture when the samples are

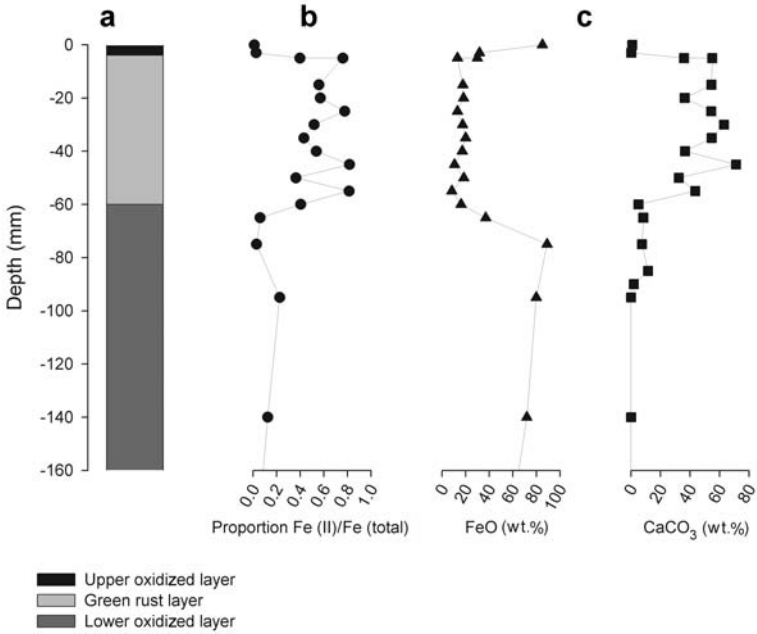

FIG. 2. Core stratigraphy and associated geochemical data: (*a*) Core stratigraphy showing the green rust layer. The core is predominantly oxidized Fe with the unusual band of dark green-black 'green rust'. (*b*) The proportion of Fe(II) with respect to Fe (total) in the core with depth. The green rust layer can be easily distinguished by the large Fe(II) content. (*c*) Weight percentage of $CaCO_3$ and FeO with depth, showing how the presence of $CaCO_3$ effectively 'dilutes' the total Fe in the green rust layer.

TABLE 1. Summary of the major chemical changes with depth through the ochre profile. This table presents an average of each layer in order to emphasize the abrupt boundaries of the green rust layer.

Depth	Description	Proportion of Fe present as Fe (II)	$CaCO_3$ (wt.%)	FeO (wt.%)
0–4 mm	Upper oxidized layer	0.01	0.9	85.0
4–20 mm	Top of green rust layer	0.44	48.5	23.1
20–40 mm	Middle of green rust layer	0.57	52.2	17.2
40–65 mm	Bottom of green rust layer	0.59	37.8	14.1
65–90 mm	Top of lower oxidized layer	0.11	9.2	68.6
90–140 mm	Middle of lower oxidized layer	0.06	0.7	66.3

freshly exposed. The lowest layer sampled, at ~210 mm depth, is a grittier, soil-like layer.

Two XRD patterns are presented in Fig. 3. The surface layer is a mixture of 2-line ferrihydrite, and more crystalline goethite (Fig. 3*a*). The 2-line ferrihydrite peak is also present in the green rust layer. Given the physicochemical parameters of the water at the Ynysarwed mine site, determined in this study, ferrihydrite will be the main mineral to precipitate (using the data from Bigham *et al.* (1996)). The oxidized layer underneath the green rust is mineralogically the same as the surface layer. The XRD patterns produced for a number of samples from the lower layers are comparable to Fig. 3*a*. The green rust sample (Fig. 3*b*) is predominantly aragonite. The additional peaks which were referenced to the powder data files (PDF) files (International Centre for Diffraction Data, 2004) and were assigned to either: pyroaurite (01-070-2150) or green rust 2 (00-052-0163). We have also compared our results to *d* spacings from previously reported XRD data on green rust (McGill *et al.*, 1975; Burke and Ferraris, 2003). Table 2 presents the interplanar spacings and intensities (relative to the most intense green rust peak) of the green rust peaks in this study together with data from green rust samples formed by the corrosion of cast iron (McGill *et al.*, 1975) and fougerite. Fougerite is an Fe/Mg green rust mineral first identified in soils by Trolard *et al.* (1997) and reported as a new mineral by Burke and Ferraris (2003).

Thermal analysis of the different layers confirms the major changes in the mineralogy. The results of DTA/TG for three representative samples are presented in Fig. 4. The upper oxidized layer is presented in Fig. 4*a*, a sample from the green rust layer is presented in Fig. 4*b* and a sample from the lower oxidized layer is presented in Fig. 4*c*. The DTA/TG patterns for the upper and lower oxidized layers are similar and confirm the presence of goethite and ferrihydrite. The patterns have been compared with ferrihydrite generated from coal mine drainage in Korea (Kim and Kim, 2003) and goethite from experimental studies (Grey *et al.*, 1983). The data presented here show endotherms at 50ºC and 275ºC for goethite and 130ºC for ferrihydrite. The green rust sample has a different pattern which confirms the presence of aragonite with a large endotherm/weight change at 920ºC and a small endotherm at 440ºC (Stolarski and Mazur, 2005). The green rust layer also shows an

TABLE 2. Interplanar spacings (Å) and relative intensities of diffraction lines from: (A) green rust formed by corrosion of cast iron (McGill *et al.*, 1975); (B) fougerite as identified by Trolard *et al.* (1997) and reported by Burke and Ferraris (2003); (C) the middle of the green rust layer in this study (20–40 mm).

A		B		C	
d (Å)	I/I_0	*d* (Å)	I/I_0	*d* (Å)	I/I_0
7.504	100	7.97	100	7.899	100
3.755	25	3.97	32	3.949	44
2.718	3	2.692	34	2.854	8
2.666	20	2.027	19	2.627	43
2.462	10	1.595	9	2.411	76
2.343	15	1.563	10	1.746	46
2.086	2			1.557	28
1.964	15				
1.74	5				
1.641	3				
1.584	5				
1.549	5				
1.462	5				

endotherm/weight loss at 180ºC which is comparable to the pattern of pyroaurite which Millange *et al.* (2000) attribute to the loss of surface and interlayer water molecules. There are no published DTA/TG patterns for green rust but pyroaurite has a similar structure to green rust (Brindley and Bish, 1976) and is, therefore, a reasonable comparison to the green rust. The chemistry of the mine drainage and the dominance of ferrihydrite/goethite in the surrounding layers suggest that the most likely mineral to form in this layer is green rust rather than pyroaurite because there is no obvious source of Mg to generate pyroaurite.

The images obtained by SEM of the green rust layer are displayed in Fig. 5. Figure 5*a* shows hexagonal crystals of green rust on a 1 μm scale with columns of hexagons also visible. The cleavage planes of the green rust are clearly visible in the hexagonal prism.

It should be noted that while previous researchers have reported a loss of identifiable green rust when air drying the sample (Phillips *et al.*, 2003*a*), our samples retain the characteristic *d* spacings of green rust which may be the result of the relatively large size of the green rust crystals reported in this study. While X-ray amorphous oxidized Fe species may have been present in the

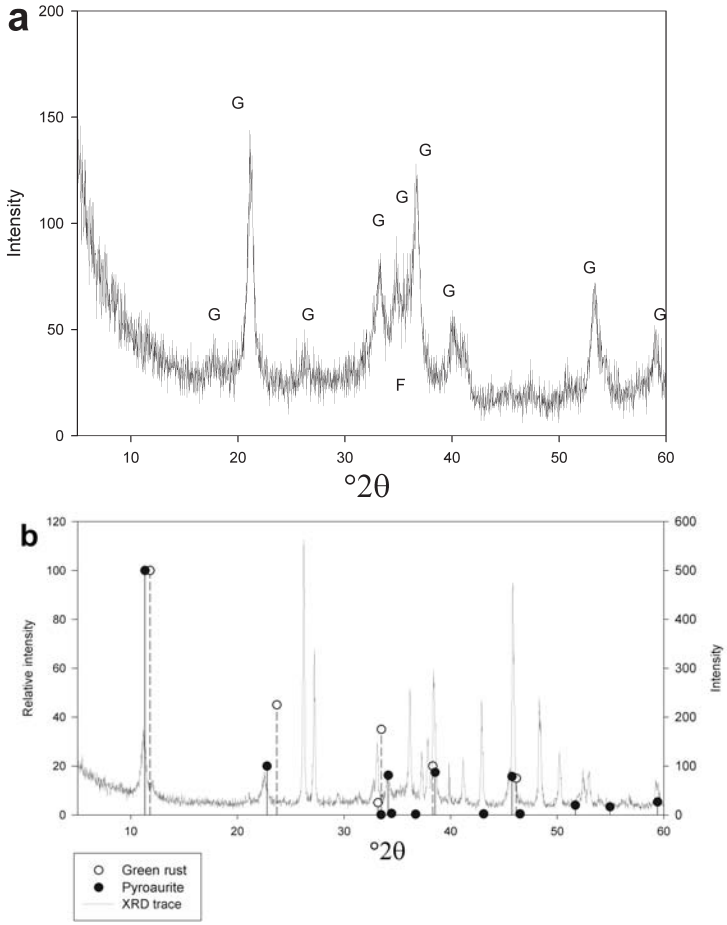

FIG. 3. XRD patterns of the core samples using Cu-*K*α radiation. The patterns are for samples from: (*a*) the top 4 mm; and (*b*) the green rust layer of the Ynysarwed adit core. The peaks in (*a*) are labelled as goethite (G) and ferrihydrite (F). The majority of the peaks in *b* can be assigned to aragonite (de Villiers, 1971) and are not labelled. Fig. 3*b* also shows open and closed circles and lines which indicate the positions and intensities of green rust and pyroaurite peaks (from the ICDD, 2004 PDF files). These peaks account for all of the peaks not assigned to aragonite.

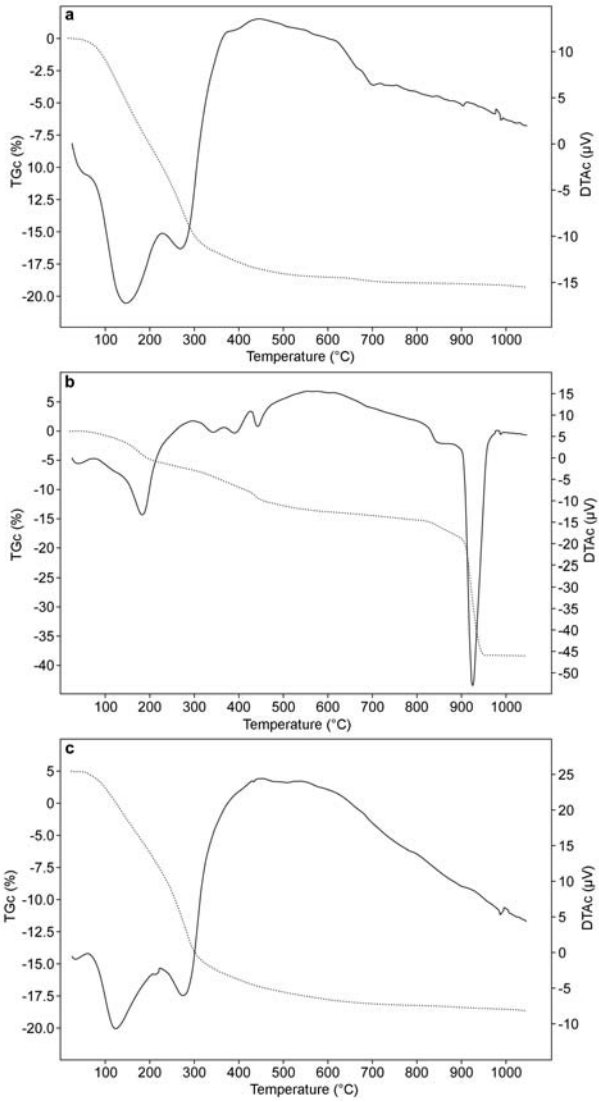

FIG. 4. DTA/TG patterns for three of the core samples. Solid lines are for DTA and dotted lines are for TG. The three diagrams are: (*a*) upper oxidized layer (0–4 mm); (*b*) the green rust layer (41–60 mm); and (*c*) the lower oxidized layer (136–172 mm). The oxidized layers (*a* and *c*) show endotherms at ~130ºC for ferrihydrite and at ~50ºC and ~275ºC for goethite. The green rust layer (*b*) shows a sharp endotherm and weight change at ~920ºC for aragonite and a weaker endotherm and minor weight change at ~180ºC comparable to that reported for pyroaurite. This endotherm is attributed to the green rust.

XRD and SEM samples, the structure of the green rust was still retained sufficiently to be identified by XRD and recognized by SEM.

Figure 5*b* shows ~30 µm long needles of aragonite which are abundant in the green rust layer. The hexagonal crystals, typical of a green rust occurrence, are also evident in this image. Aragonite was only found in the green rust layer which suggests that the formation of green rust, at this location, is linked to the generation of aragonite. The chemical profile of the core (Fig. 2) shows that the $CaCO_3$ content of the material drops dramatically below the green rust layer. The aragonite crystals are, therefore,

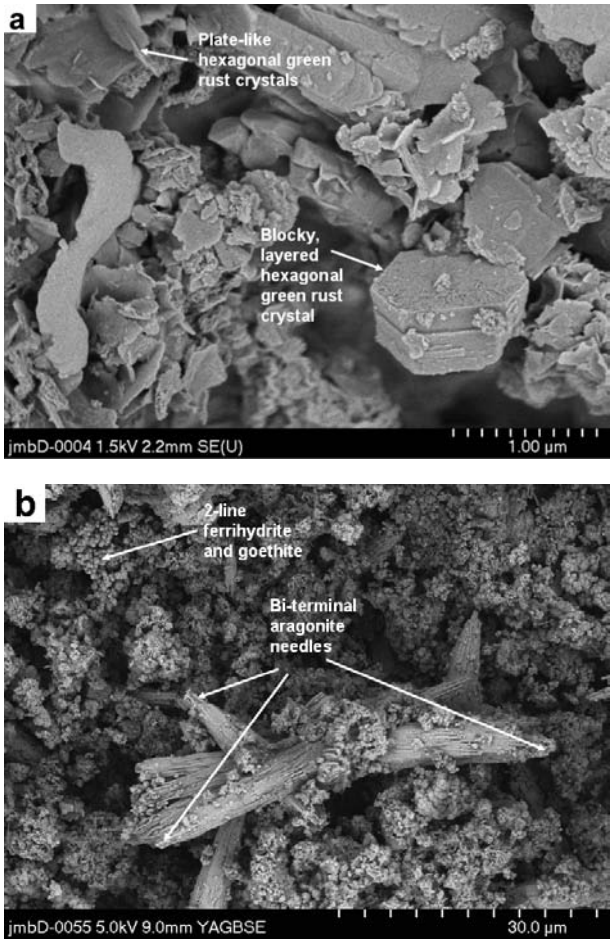

FIG. 5. SEM images of green rust showing: (*a*) secondary electron image, with accelerating voltage of 1.5 kV and a working distance of 2.2 mm, of the characteristic hexagonal crystals of green rust. Both blocky and plate-like hexagonal crystals are indicated on the SEM image; and (*b*) back-scattered electron image with 5.0 kV accelerating voltage and 9.0 mm working distance, of needles of aragonite abundant in the sample surrounded by amorphous material and clusters of blocky hexagonal green rust crystals.

restricted to the green rust layer. Figure 2 also shows the profile of Fe(II) as a proportion of total Fe with depth. In the green rust layer the Fe(II) proportion is ~0.6. Green rust with the stoichiometric formula given above should have an Fe(II) proportion of 0.66. The slightly lower value could result from either rapid oxidation of the material on exposure to the air or from a non-stoichiometric ratio (as described by Schwertmann and Cornell, 2000). The green rust layer is easily distinguished graphically because above and below the green rust layer the Fe is predominantly oxidized, with a proportion of Fe(II) of <0.1. Figure 2 also demonstrates how total Fe displayed as FeO decreases in the green rust layer; this is contrasted by an increase in the Ca content expressed as $CaCO_3$. The presence of aragonite 'dilutes' the Fe content of the green rust layer.

Today the Ynysarwed mine site produces a water flow of ~30 l s^{-1} (Evans *et al*., 2006). The chemistry of the mine drainage determined in this study shows distinct changes compared with the results quoted by Ranson (1999). The pH is typically ~6, the dissolved oxygen is measured as 1.6 mg l^{-1} and the water contains ~90 mg l^{-1} Fe. Other measured parameters include an Eh of

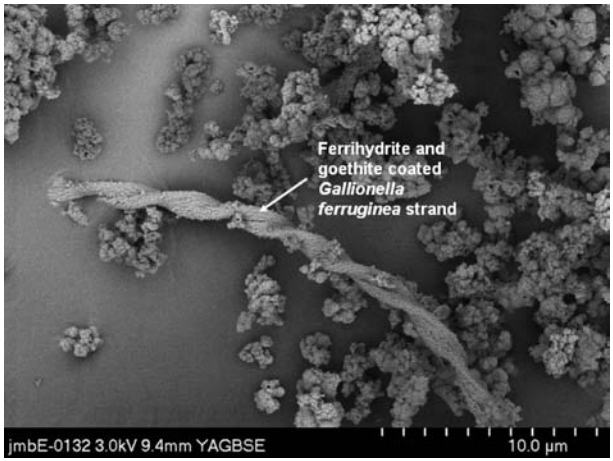

FIG. 6. Back-scattered electron micrograph, with accelerating voltage of 3.0 kV and a working distance of 9.4 mm, of a *Gallionella ferruginea* stalk which is encrusted in ferrihydrite and goethite. This specimen was taken from the upper oxidized layer of the core.

6 mV, a conductivity of 2000 µS cm^{-1} and Ca, SO_4 and HCO_3 concentrations of 150, 1082 and 81 mg l^{-1} respectively. These parameters have important implications for the generation of 2-line ferrihydrite and the green rust/aragonite layer at this site.

The low levels of dissolved oxygen in the Ynysarwed drainage, measured in this study, mean that inorganic oxidation of the dissolved Fe, to generate the ferrihydrite, is unlikely. The precipitation of the ochre from this reduced water is attributed to the presence of *Gallionella ferruginea* (Anesio, pers. comm. 2006) which is an Fe-oxidizing bacteria with 'numerous helically wound, uniquely mineralized fibrils [extending] outward from the convex side' (Ridgeway *et al.*, 1981). This stalk structure protrudes from the concave side of the cell, and is dependent on population development, pH, and redox conditions. These stalks are generally covered in bacteriogenic Fe oxide precipitate which gives it a reddish-brown colour (Anderson and Pedersen, 2003). Figure 6 is an SEM image showing the remains of a strand of *Gallionella ferruginea* coated by amorphous ferrihydrite and goethite. The *Gallionella* were identified within the upper ferrihydrite layer.

Summary

To the authors' knowledge the Ynysarwed coal mine drainage site is the first recorded occurrence of green rust found in ochreous mine discharges. It has been identified by the stoichiometric Fe(II)/Fe(III) ratio, hexagonal crystal form and XRD charactersitics. The close association of green rust and aragonite suggests that the origin of these two minerals is interrelated. This new mode of occurrence contains much more extensive green rust development than other environments in which it has been described.

Acknowledgements

The authors wish to thank Alex Anesio (Institute of Biological Sciences, Aberystwyth) for his help with the identification of the *Gallionella* in the SEM images. We also thank Karen Hudson-Edwards and an anonymous referee for their constructive reviews.

References

Anderson, C.R. and Pedersen, K. (2003) *In situ* growth of *Gallionella* biofilms and partitioning of lanthanides and actinides between biological material and ferric oxyhydroxides. *Geobiology Journal*, **1**, 169–178.

Bigham, J.M., Schwertmann, U., Traina, S.J., Winland, R.L. and Wolf, M. (1996) Schwertmannite and the chemical modelling of iron in acid sulfate water. *Geochimica et Cosmochimica Acta*, **60**, 2111–2121.

Bond, D.L. and Fendorf, S. (2003) Kinetics and structural constraints of chromate reduction by green

rusts. *Environmental Science and Technology*, **37**, 2750–2757.

Bourrie, G., Trolard, F., Refait, P. and Feder, F.R. (2004) A solid-solution model for Fe(II)-Fe(III)-Mg(II) green rusts and fougerite and estimation of their Gibbs free energies of formation. *Clays and Clay Minerals*, **52**, 382–394.

Brindley, G.W. and Bish, D.L. (1976) Green rust: a pyroaurite type structure. *Nature*, **263**, 353.

Burke, E.A.J. and Ferraris, G. (2003) New minerals approved in 2003 and nomenclature modifications approved in 2003 by the Commission on New Minerals and Mineral Names, International Mineralogical Association. *American Mineralogist*, **89**, 1566–1573.

Choe, S., Liljestrand, H.M. and Khim, J. (2004) Nitrate reduction by zero-valent iron under different pH regimes. *Applied Geochemistry*, **19**, 335–342.

De Villiers, J.P.R. (1971) Crystal structures of aragonite, strontianite witherite. *American Mineralogist*, **56**, 758–767

Drissi, S.H., Refait, M., Abdelmoula, M. and Genin, J.M.R. (1995) The preparation and thermodynamic properties Fe(II)-Fe(III) hydroxide-carbonate (green rust 1); pourbaix diagram of iron in carbonate-containing aqueous media. *Corrosion Science*, **37**, 2025–2041

Evans, K.A., Watkins, D.C. and Banwart, S.A. (2006) Rate controls on the chemical weathering of natural polymineralic material II. Rate controlling mechanisms and mineral sources and sinks for element release from four UK mine sites, and implications for comparison of laboratory and field scale weathering studies. *Applied Geochemistry*, **21**, 377–403.

Genin, J.M.R. (2004) Fe(II-III) hydroxysalt green rusts; from corrosion to mineralogy and abiotic to biotic reactions by Mossbauer spectroscopy. *Hyperfine Interactions*, **156**, 445–451.

Grey, I.E., Li, C. and Watts, J.A. (1983) Hydrothermal synthesis of goethite-rutile intergrowth structures and their relationship to pseudorutile. *American Mineralogist*, **68**, 981–988.

Guion, P.D., Gutteridge, P. and Davies, S.J. (2000) Carboniferous sedimentation and volcanism on the Laurussian margin. Pp. 227–230 in: *Geological History of Britain and Ireland* (N. Woodcock and R. Strachan editors). Blackwell Science, Oxford, UK.

Hansen, H.C.B., Koch, C.B., Nancke-Krogh, H., Borggaard, O.K. and Sørensen, J. (1996) Abiotic nitrate reduction to ammonium: key role of green rust. *Environmental Science and Technology*, **30**, 2053–2056.

Jiang, J.H., Dempsey, B.A., Catchen, G.L. and Burgos, W.D. (2003) Effects of Zn(II), Cu(II), Mn(II), Fe(II), NO_3^-, or SO_4^{2-} at pH 6.5 and 8.5 on transformations of hydrous ferric oxide (HFO) as evidenced by Mössbauer Spectroscopy. *Colloids and Surfaces A – Physicochemical and Engineering Aspects*, **221**, 55–68.

Kamolpornwijit, W., Liang, L.Y., Moline, G.R., Hart, T. and West, O.R. (2004) Identification and quantification of mineral precipitation in Fe^0 filings from a column study. *Environmental Science and Technology*, **38**, 5757–5765.

Kim, J.J. and Kim, S.J. (2003) Mineralogy of ferrihydrite and schwertmannite from the acid mine drainage in the Donghae coal mine area. *Journal of the Mineralogical Society of Korea*, **16**, 191–198.

Koch, C.B. and Mørup, S. (1991) Identification of green rust in an ochre sludge. *Clay Minerals*, **26**, 577–582.

Kohn, T., Livi, K.J.T., Roberts, A.L. and Vikesland, P.J. (2005) Longevity of granular iron in groundwater treatment processes: Corrosion product development. *Environmental Science and Technology*, **39**, 2867–2879.

McCleskey, R.B., Nordstrom, D.K. and Maest, A.S. (2004) Preservation of water samples for arsenic (III/V) determinations: An evaluation of the literature and new analytical results. *Applied Geochemistry*, **19**, 995–1009.

McGill, I.R., McEnaney, B. and Smith, D.C. (1975) Crystal structure of green rust caused by corrosion of cast iron. *Nature*, **259**, 200–201.

Millange, F., Walton, R.I. and O'Hare, D. (2000) Time-resolved in situ X-ray diffraction study of the liquid-phase reconstruction of Mg-Al-carbonate hydrotalcite-like compounds. *Journal of Materials Chemistry*, **10**, 1713–1720

Ona-Nguema, G., Carteret, C., Benali, O., Abdelmoula, M., Genin, J.M. and Jorand, F. (2004) Competitive formation of hydroxycarbonate green rust 1 versus hydroxysulphate green rust 2 in Shewanella putrefaciens cultures. *Geomicrobiology Journal*, **21**, 79–90.

O'Loughlin, E.J., Kelly, S.D., Kemner, K.M., Csencsits, R. and Cook, R.E. (2003) Reduction of Ag-I, Au-III, Cu-II and Hg–II by Fe-II/Fe-III hydroxysulfate green rust. *Chemosphere*, **53**, 437–446.

Phillips, D.H., Gu, B., Watson, D.B. and Roh, Y. (2003*a*) Impact of sample preparation on mineral analysis of zero-valent iron reactive barrier materials. *Journal of Environmental Quality*, **32**, 1299–1305.

Phillips, D.H., Watson, D.B., Roh, Y. and Gu, B. (2003b) Mineralogical characteristics and transformations during long-term operation of a zerovalent iron reactive barrier. *Journal of Environmental Quality*, **32**, 2033–2045.

Ranson, C.M. (1999) Minewater treatment in Neath Port Talbot. *Proceedings of the Institution of Civil Engineers Municipal Engineer*, **133**, 183–193.

Refait, P., Abdelmoula, M., Trolard, F., Genin, J.M.R., Ehrhardt, J.J. and Bourrie, G. (2001) Mössbauer and

XAS study of a green rust mineral; the partial substitution of Fe^{2+} by Mg^{2+}. *American Mineralogist*, **86**, 731–739.

Refait, P., Benali, O., Abdelmoula, M. and Genin, J.M.R. (2003) Formation of 'ferric green rust' and/or ferrihydrite by fast oxidation of iron (II-III) hydroxychloride green rust. *Corrosion Science*, **45**, 2435–2449.

Ridgway, H.F., Means, E.G. and Olson, B.H. (1981) Iron bacteria in drinking-water distribution-systems – elemental analysis of *Gallionella* stalks, using X-ray energy-dispersive microanalysis. *Applied and Environmental Microbiology*, **41**, 288–297

Ruby, C., Upadhyay, C., Géhin, A., Ona-Nguema, G. and Génin, J.-M. R. (2006) In situ redox flexibility of Fe II-III oxyhydroxycabonate green rust and fougerite. *Environmental Science and Techonology*, **40**, 4696–4702.

Schwertmann, U. and Cornell, R.M. (2000) *Iron Oxides in the Laboratory; Preparation and Characterization*, 2nd edition. Wiley-VCH, Weinheim, Germany.

Stampfl, P.P. (1969) A basic iron (II,III)-carbonate formed during corrosion. *Corrosion Science*, **9**, 185–187

Stolarski, J. and Mazur, M. (2005) Nanostructure of biogenic versus abiogenic calcium carbonate crystals. *Acta Palaeontologica Polonica*, **50**, 847–865.

Taylor, H.F.W. (1973) Crystal-structures of some double hydroxide minerals. *Mineralogical Magazine*, **39**, 377–389

Trolard, F., Génin, J.-M.R., Abdemoula, M., Bourrié, G., Humbert, B. and Herbillion, A. (1997) Identification of a green rust mineral in a reductomorphic soil by Mössbauer and Raman spectroscopies. *Geochemica et Cosmochimica Acta*, **61**, 1107–1111.

Wilkin, R.T. and McNeil, M.S. (2003) Laboratory evaluation of zero-valent iron to treat water impacted by acid mine drainage. *Chemosphere*, **53**, 715–725.

Wilson, A.D. (1955) A new method for the determination of ferrous iron in rocks and minerals. *Bulletin of the Geological Survey of Great Britain*, **9**, 55–58.

[*Manuscript received 1 January 2007: revised 15 February 2007*]